

Prediction of hot tear formation in vertical DC casting of aluminum billets using a granular approach

M. Sistaninia¹, J.-M. Drezet¹, A.B. Phillion², M. Rappaz¹

1. Computational Materials Laboratory, Ecole Polytechnique Fédérale de Lausanne, Lausanne, Switzerland

2. School of Engineering, University of British Columbia Okanagan, Kelowna, Canada

Abstract

A coupled hydro-mechanical granular model aimed at predicting hot tear formation and stress-strain behavior in metallic alloys during solidification is applied to the semi-continuous direct chill casting of aluminum alloy round billets. This granular model consists of four separate 3D modules: (i) a solidification module that is used for generating the solid-liquid geometry at a given solid fraction; (ii) a fluid flow module that is used to calculate the solidification shrinkage and deformation-induced pressure drop within the intergranular liquid; (iii) a semi-solid deformation module that is based on a combined finite element / discrete element method and simulates the rheological behavior of the granular structure; and (iv) a failure module that simulates crack initiation and propagation. To investigate hot tearing, the granular model has been applied to a representative volume within the direct chill cast billet that is located at the bottom of the liquid sump, and reveals that semi-solid deformations imposed on the mushy zone open the liquid channels due to localization of the deformation at grains boundaries. At a low casting speed, only individual pores are able to form in the widest channels since liquid feeding remains efficient. However, as the casting speed increases, the flow of liquid required to compensate for solidification shrinkage also increases and as a result the pores propagate and coalesce to form a centerline crack.

1. Introduction

The formation of hot tears along the center line of round billets is a serious flaw in semi-continuous vertical direct chill (DC) casting of aluminum alloys. Although grain refinement helps to reduce the initiation of cracks [1, 2], this defect still appears at high casting speed thus limiting the productivity of the process.

Modeling hot tear formation requires a multi-scale approach that takes into account both fluid flow within the thin intergranular liquid films present between growing and coalescing grains of the mushy zone, and macroscopic thermal and mechanical loadings imposed by the rest of the casting. The hydro-mechanical coupled model for solidification and semi-solid deformation [3-5], recently developed by our research group, uses a granular approach to fulfill the above requirements and simulate hot tearing. The use of a granular approach enables each grain to exist as a discrete element while allowing for efficient simulation of an ensemble of grains making up the microstructure. The deformation predictions obtained from this model were validated against experimental tensile test data acquired from semi-solid aluminum alloys [5]. In the present work, the hydro-mechanical coupled granular model is used to predict the formation of hot tearing in an industrial aluminum alloy, AA5182, during semi-continuous DC casting of round billets.

The model consists of four separate 3D modules: (i) a Solidification Module (SM) for generating the solid-liquid geometry at a given solid fraction, (ii) a Fluid Flow Module (FFM) for liquid flow and the pressure drop calculation, (iii) a Semi-solid Deformation Module (SDM) for localization of straining and (iv) a Failure Module (FM) for modeling fracture development. Since solid deformation, intergranular flow, and crack initiation are deeply linked together, the FFM, SDM, and FM are coupled. This is achieved by carrying out each of the FFM, SDM, and FM simulations incrementally at a given fraction of solid, with iterations between each increment, until bulk fracture occurs. For further information on the modeling methodology please refer to [3-5].

One of the main differences between experimental studies and industrial occurrences of hot tearing is the crack initiation site. During semi-solid deformation tests, cracks form on the cast surface since ambient air can fill the growing cavity of the crack. In this situation, the criterion for crack formation is based on the overpressure required to overcome the capillary forces at the liquid-gas interface [5, 6] and thus a hot tear will form once the liquid pressure in a channel is such that

$$p_\ell^c = p_g - \frac{\lambda \cos \Theta}{h} \quad (1)$$

where p_g is the gas pressure, Θ is the dihedral angle, λ the surface tension at the gas-liquid interface, and h is the half-width of the liquid channel. During DC casting, however, hot tears initiate in the center of the billet. In this situation, the mushy zone is surrounded on the sides and the bottom by a fully solid medium and on the top by the liquid pool. Thus, ambient air cannot provide the gas required for filling the cavity of the crack. As shown in [7], the fracture surfaces of hot tears in DC cast billets do not contain a surface oxide film. The formation of a hot tear in the center of the billet, without the presence of ambient air, poses a dilemma for researchers. While the liquid pressure required to form a crack in a gas-free liquid by breaking the bonds between the molecules is extremely low, on the order of ~ 670 MPa [8], the maximum strength of semi-solid alloys at high temperature is only a few MPa. This large difference in pressures makes it impossible for cracks to form directly in a gas-free liquid (since the vapor pressure of Al near its melting point as well as that of most solute elements is also very low). It seems that gas dissolved in the melt, mainly hydrogen in the case of aluminum, is the reason for this discrepancy and accordingly plays an important role in hot tearing formation.

As is well known, hydrogen solubility is much smaller in the solid phase as compared to the liquid, resulting in an increase during solidification of the hydrogen content within the liquid. Fig. 1 shows the evolution of the hydrogen composition in the liquid phase of an AA5182 alloy as a function of fraction solid (dashed line), along with the equilibrium saturation content, $C_{g\ell}^{eq}$ [9] (solid line). The hydrogen evolution has been calculated from the equilibrium partition coefficient, $k_{0g} = C_{gs}/C_{g\ell}$, and assuming an initial composition of $0.1 \text{ cc}_{\text{stp}}/100 \text{ g}^1$. At fractions of solid above $g_s \sim 0.75$, $C_{g\ell}^{eq} < C_{g\ell}$ and so the melt is supersaturated with respect to hydrogen, thus enabling porosity formation.

Commet et al. [7] investigated hot tear initiation during DC casting of AA5182 round billets as a function of casting velocity using ultra-sound techniques. Fig. 2 shows the evolution in morphology of a hot tear with increasing casting speed, v_T [10]. The images depict the defect formation in a cross-section of a DC cast billet. At low v_T , i.e. solidification velocities² less than 90 mm/min for a given billet diameter, hot tearing does not occur. As v_T is increased, porosity is found in an annular distribution around the center. With further increase of v_T , a rather linear macro-crack (hot tear) is observed to form. Finally, as the solidification velocity approaches 120 mm/min , the tear develops into a star-shaped crack with three branches. These industrial results confirm

¹ $0.1 \text{ cc}_{\text{stp}}/100 \text{ g}$ corresponds to 0.1 cubic centimeter of gas under standard temperature and pressure per 100 g of metal.

² On the centerline axis of the DC cast round billet, solidification velocity, v_T , and casting speed are equal.

experimental findings by Phillion et al.[11] who performed semi-solid tensile tests on AA5182 specimens that were both in the as-cast (i.e. with porosity) and hot isostatic pressed state (i.e. without porosity) and concluded that porosity formation is a necessary condition for hot tearing.

The hydro-mechanical coupled granular model outlined above has provided much new insight into hot tear formation. For example, this model predicts [5] that hot tearing formation is a function of both the imposed strain and strain rate on the mushy zone during solidification, as reported experimentally [1]. In the following sections, we first provide a qualitative validation of the failure model against experimental results showing crack propagation during semi-solid deformation in Al-Cu alloys, and then second apply the model to predict hot tearing during industrial DC casting of AA5182 round billets.

2. Validation of the Failure Model via X-ray tomographic imaging

The experimental data for validation of the failure model was acquired during tensile testing of an Al-Cu alloy in the semi-solid state. In this work, the tensile testing was combined with *in-situ* X-ray microtomography at ESRF [12] to acquire a real-time 3D image of crack propagation from tensile deformation. To ensure that the deformation was captured in the field-of-view of the X-ray detector, the cross-section of the specimen was locally reduced at the center to localize the tensile deformation. At the beginning of the test, the specimen was heated up to 828 K, which corresponds to $g_s \sim 0.91$ based on the lever rule. After a three-minute hold time, the tensile test was initiated at a deformation rate of $V_d = 0.1 \mu\text{ms}^{-1}$ and X-ray radiographs were recorded for reconstruction into 3D images. Al-Cu is a good model system since the Cu-rich liquid has considerably greater X-ray attenuation as compared with the primary solid grains. Consequently, all three phases (liquid, solid, pore) can be easily observed in the tomographic images.

The corresponding granular model results assume that there is contact between the intergranular liquid and atmosphere. Considering that a thin oxide skin forms between the liquid and atmosphere, the value of $\lambda \cos \Theta$ in Eq.1 is fixed to 5 J m^{-2} [5, 6]. Also, the average grain size is assumed to be $200 \mu\text{m}$, while the physical parameters used in the computations are given in [5]. Fig. 3 shows a qualitative comparison of the evolution in the semi-solid microstructure during the tensile deformation between (a) predictions of the granular model and (b) observations via X-ray tomography [12] at three different times of deformation. The deformation is in the vertical direction and downward. The contour plots shown in Fig. 3(a) also provide an indication of the maximum principal strain in a cross-section containing the centerline axis. The black channels correspond to those where a hot tear has formed.

As can be seen by comparing Fig. 3(a) and Fig. 3(b), strain localization is concentrated within the liquid films located between the grains. The maximum local strain is predicted to be about two orders of magnitude larger than the bulk strain of the domain, i.e. $\epsilon = V_r \times t/L$ ($L=2$ mm refers to the length of the domain). During tensile testing, liquid flows from less deformed zone towards the notched zone in order to accommodate the deformation (i.e., drainage of liquid towards the most highly deformed region). It would also appear that, considering all the assumptions, the model provides a good representation of crack formation during semi-solid deformation as the accumulation of liquid and the void propagation in the notched zone predicted by the granular model is also clearly observed in the tomography images.

3. Application of the Granular Model to hot tear formation in DC casting of round billets

The utility of the granular model is to explore the behavior of the mushy zone of industrial casting scenarios where hot tear formation is prevalent and thus limits quality and productivity, such as during the DC casting of the AA5182 alloy [7]. To study hot tearing in DC casting, we have considered only the regime at high fraction of solid ($0.92 < g_s < 0.95$), since this is where hot tears are known to initiate. The granular model required two major modifications as compared with the validation exercise presented in Section 2. First, since the granular model was developed for binary alloys [13], the physical properties (partition coefficient, k_0 , eutectic temperature, T_{eut} , solute composition, C_0 and slope of liquidus line, m_l) were modified such that the evolution of the solid fraction with temperature within the representative volume was in agreement with the solidification path reported for the AA5182 alloy [10]. As can be seen in Fig. 4, good agreement is found between the two curves in the region at high fraction of solid that is of interest for hot tearing. The corresponding physical property data, along with other properties used in the simulations, are provided in Table 1. Second, the value of $\lambda \cos\theta$ was determined through a trial and error process so that the model predicts hot tear formation under conditions that are known from the work of Commet et al. [7] to lead to hot tearing. A good agreement was found with $\lambda \cos\theta = 0.26 \text{ N m}^{-1}$.

To examine hot tear formation during DC casting using the granular model, the solidification and semi-solid deformation of a representative volume of semi-solid metal located at the center of the billet is studied using the granular model at two different casting speeds (90 mm/min and 120 mm/min). The tensile deformation imposed to the representative volume is assumed to be independent of casting speed and consequently a strain rate of $\dot{\epsilon} = 2 \times 10^{-4} \text{ s}^{-1}$ was applied to both simulations. The size of the domain is a parallelepipedon with dimensions $1.8 \times 1.8 \times 6 \text{ mm}^3$ and containing 2430 grains, i.e., an average grain size of about 200 μm , as shown in Fig. 5(a). The temperature on the surface $z = 0$ is 548°C; it decreases to 510°C on the surface $z = L_z = 6$ mm resulting in a constant

thermal gradient of $G_T = 5000^\circ\text{C}/\text{m}$ (L_x , L_y and L_z refer to the length of the domain in the X, Y, and Z directions, Z being the axis of the billet).

Based on the solidification module, the average solid fraction is $g_{s,\max} = 0.95$ at $z = 0$ and $g_{s,\min} = 0.92$ at $z = L_z$. For the semi-solid deformation module, a symmetry boundary condition is applied to the surfaces $x = 0$ and $y = -L_y$ while the surfaces $x = L_x$ and $y = 0$ are connected to two reference nodes that are displaced at a fixed velocity corresponding to the imposed strain rate along X and Y directions. The surface $z = L_z$ is free to move and the surface $z = 0$ is constrained along Z. The use of a reference node enables the bulk semi-solid constitutive behavior to be obtained directly from the force–displacement curve predicted at this location. For the fluid-flow module, liquid metal will flow from the surface $z = L_z$ to $z = 0$ because of the variation in fraction of solid that occurs between these surfaces. In order to feed the representative volume, the liquid metal must first traverse a mushy zone that is exterior to the representative volume and is at higher temperature and consequently at lower g_s . The corresponding boundary condition for the surface $z = L_z$ is the so-called Robin condition,

$$v_\ell = f_\ell(p_\ell - p_m) \quad (2)$$

where v_ℓ is the microscopic liquid velocity, f_ℓ the feeding coefficient [5] and p_m the metalostatic pressure at $g_s = 0$. Using Darcy's law to approximate fluid flow in the mushy zone exterior to the representative volume, f_ℓ at the surface $z = L_z$ is calculated to be $2 \times 10^{-2} \mu\text{m Pa}^{-1} \text{s}^{-1}$. Assuming that ρ_ℓ , ρ_s and v_T are uniform across the mushy zone, the average velocity of the liquid leaving the domain through the surface $z = 0$ to feed the solidification shrinkage of the partial mushy zone between $g_{s,\max} < g_s < 1$ is given by $v_\ell = \beta v_T (1 - g_{s,\max})$. This flux is imposed on the surface $z = 0$. Finally, all the other surfaces are closed to fluid flow.

Figure 6 shows pressure contour plots within the domain at three different strains corresponding to different times of deformation for $v_T = 120 \text{ mm}/\text{min}$. The solid and liquid phases on the upper half of the domain are transparent to display the crack propagation within the domain. The channels that are not transparent within the upper half of the domain are those where a crack has formed. As deformation proceeds, the thickness of the liquid channels increases and thus their resistance to hot tearing formation decreases according to the Eq. (1). Consequently, the size of the crack increases with deformation. Figure 7 shows pressure contour plots within the domain at three different strains for $v_T = 90 \text{ mm}/\text{min}$ and $\dot{\epsilon} = 0.0002 \text{ s}^{-1}$. Although a few individual pores form in a few wide channels, which are not visible in this figure, they do not propagate and thus hot tear formation is not predicted.

Comparing Fig. 6 with Fig.7, the present model predicts that the hot tearing sensitivity in DC casting increases with increasing casting speeds in agreement with experimental data as shown in Fig. 2, and industrial practice. By adjusting only one parameter, $\lambda \cos\theta$, the present model is able to distinguish safe casting conditions from conditions that will lead to the formation of centerline hot tears.

4. Conclusion

The present granular model based on a coupling between solidification, fluid flow, semi-solid deformation and crack initiation is able to predict centerline hot tearing formation in vertical DC casting of round billets. The effects of casting speed, strain and strain rate acting over the mushy zone are all well retrieved by the model. Due to the localization of straining, the thickness of the liquid channels increases as deformation proceeds and consequently their resistance to hot tearing formation decreases. Because of that, strain besides strain rate plays an important role in hot tearing formation. By adjusting only one parameter, the model appears to be fully predictive.

5. References

1. D.G. Eskin, Suyitno, and L. Katgerman, *Prog. Mater. Scien.*, 2004, Vol. 49, pp. 629-711.
2. S. Li, K. Sadayappan, and D. Apelian, *Metall. Mater. Trans. B*, 2013, Vol., pp. 1-10.
3. M. Sistaninia, A.B. Phillion, J.M. Drezet, and M. Rappaz, *Metall. Mater. Trans. A*, 2011, Vol. 42, pp. 239-48.
4. M. Sistaninia, A.B. Phillion, J.M. Drezet, and M. Rappaz, *Acta Mater.*, 2012, Vol. 60, pp. 3902-11.
5. M. Sistaninia, A.B. Phillion, J.M. Drezet, and M. Rappaz, *Acta Mater.*, 2012, Vol. 60, pp. 6793-803.
6. M. Sistaninia, S. Terzi, A.B. Phillion, J.M. Drezet, and M. Rappaz, *Acta Mater.*, 2013, Vol. 61, pp. 3831-41.
7. B. Commet, P. Delaire, J. Rabenberg, and J. Storm, in *Light Metals 2003*. San Diego, CA; United States: TMS, Warrendale, PA.
8. J. Hoyt and A. Potter, *Metall. Mater. Trans. A*, 2012, Vol. 43, pp. 3972-7.
9. J.A. Dantzig and M. Rappaz, *Solidification*. 2009, Lausanne: EPFL Press.
10. P.D. Grasso, *Coalescence and mechanical behaviour of semi-solid aluminium alloys in relation to hot tearing*, PhD thesis, 2004, EPFL.
11. A.B. Phillion, S. Thompson, S.L. Cockcroft, and M.A. Wells, *Mater. Scien. Engin. A*, 2008, Vol. 491, pp. 237-47.
12. S. Terzi, L. Salvo, M. Suéry, A. Dahle, and E. Boller, *Trans. Nonferrous Metals Society of China*, 2010, Vol. 20, Supplement 3, pp. s734-s8.
13. A.B. Phillion, J.L. Desbiolles, and M. Rappaz, in *Modeling of Casting, Welding, And Advanced Solidification Processes - XII*. Minerals, Metals & Materials Soc, 184 Thorn Hill Rd, Warrendale, Pa 15086-7514 Usa.

Table 1. physical properties used for the granular simulation

β	0.08	k_0	0.1
G	5000 [C/m]	C_0	0.5 [at%]
$\lambda \cos \theta$	0.26 [N/m]	T_{eut}	550 [°C]
μ_ℓ	1.5e-3 [Pa/s]	m_ℓ	-20 [K/at%]

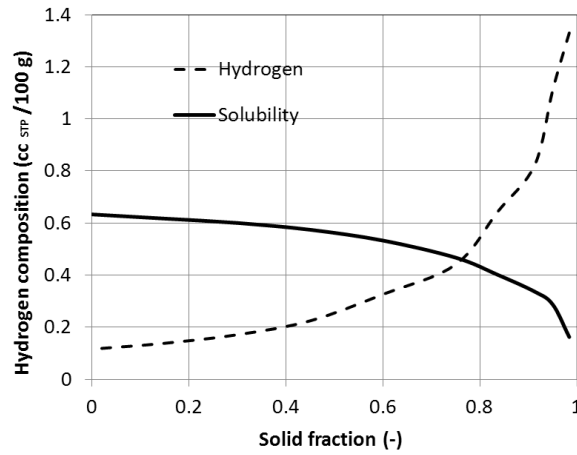


Fig. 1 Evolution of the hydrogen content in the liquid as a function of the fraction of solid, along with the equilibrium hydrogen saturation content for an AA5182 aluminum alloy. The initial composition was 0.1 cc_{stp}/100 g.

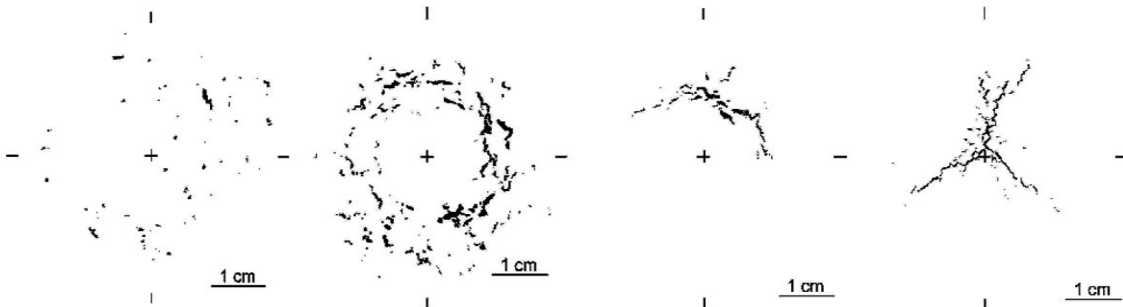


Fig. 2 Evolution of the hot tear morphology due to the increase in v_T from 90 mm/min to 120 mm/min. The center of the billet is indicated by the cross[10].

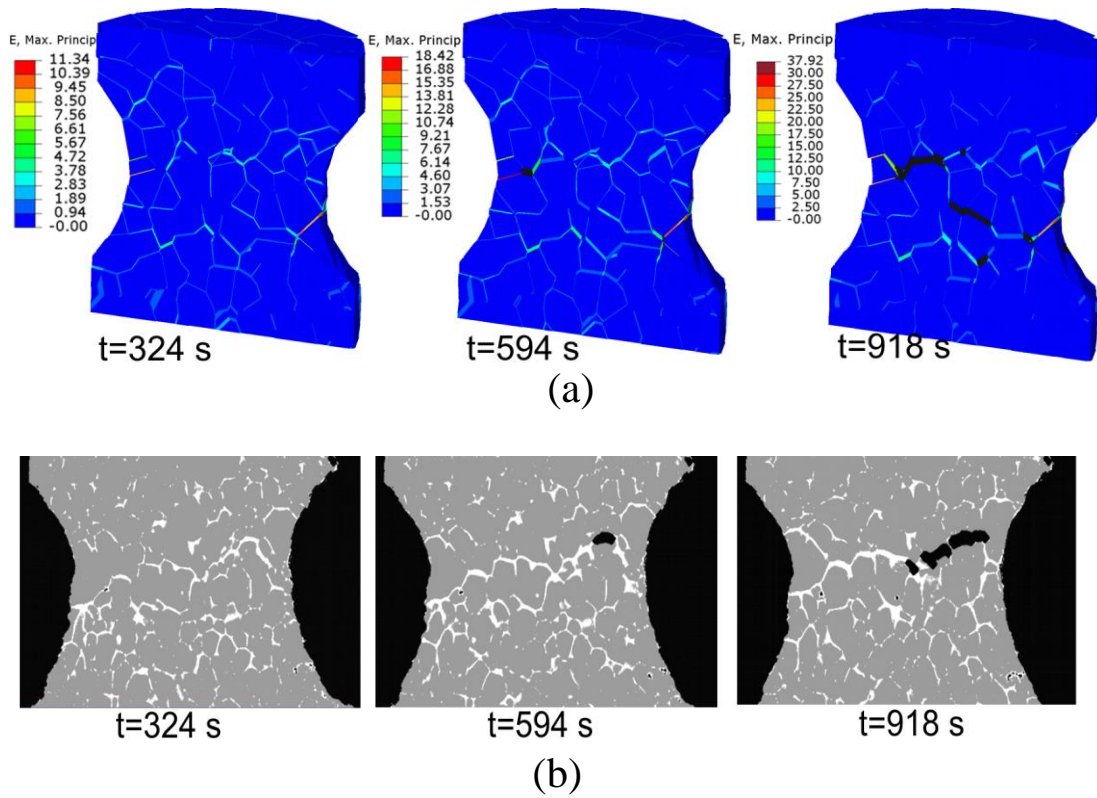


Fig. 3 Comparison of the evolution in semi-solid microstructure during tensile deformation as (a) predicted by the granular model and (b) observed by X-ray tomography [7] at three different times of deformation. The isothermal tensile tests were conducted at a fraction of solid of 0.91.

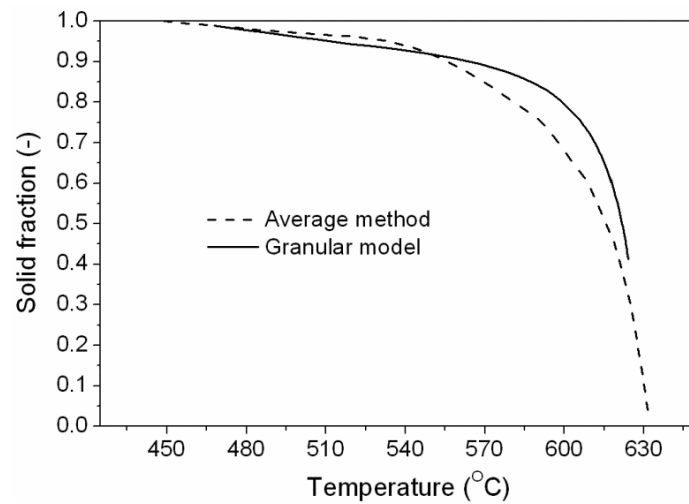


Fig. 4 Evolution of solid fraction with temperature as calculated with the granular model and reported in Ref.[10].

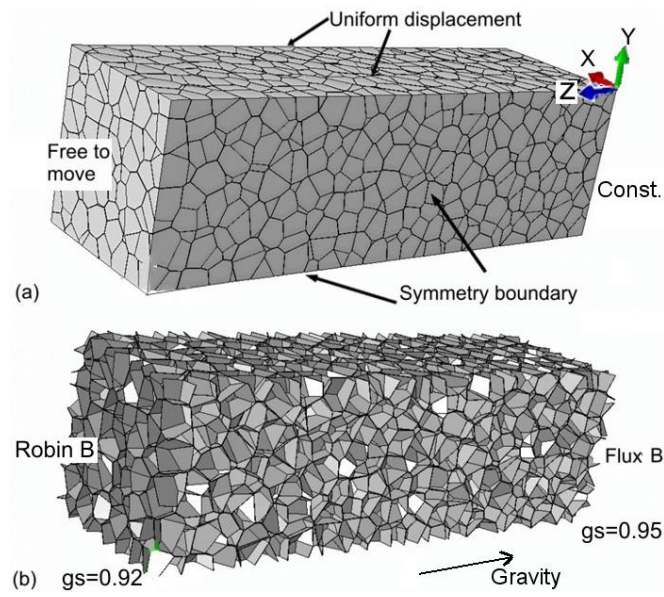


Fig. 5 Boundary conditions applied to the semi-solid RVE containing 2430 grains for (a) SDM calculation and (b) FFM calculation. The solid elements are transparent in (b) in order to see the liquid film network in-between the polyhedral grains.

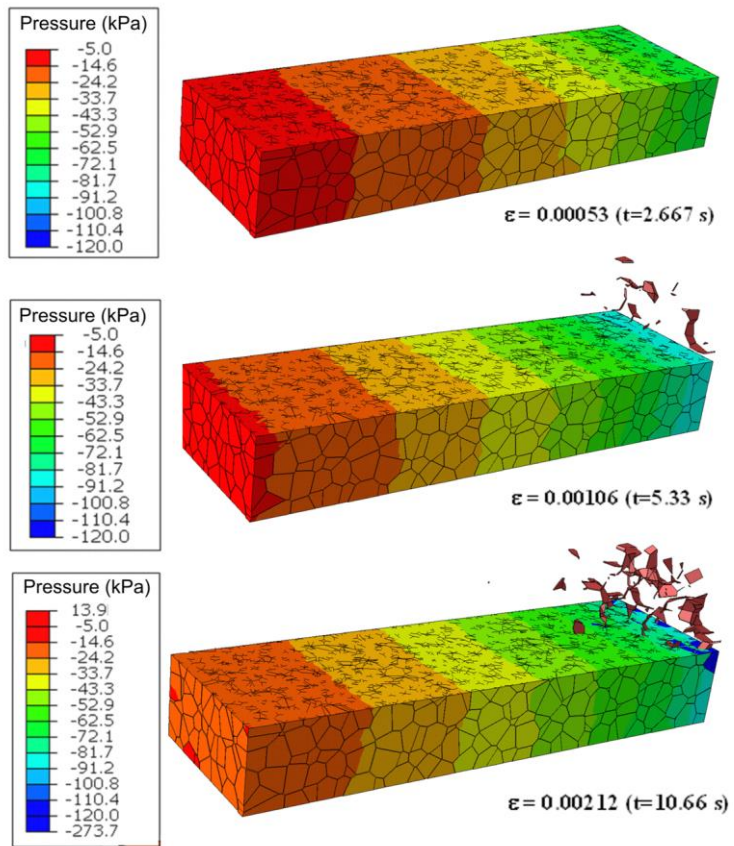


Fig. 6 Contour plots of the liquid pressure for $v_T=120$ mm/min and $\dot{\epsilon} = 0.0002$ s⁻¹ at three different strains. The time of deformation is given in parentheses.

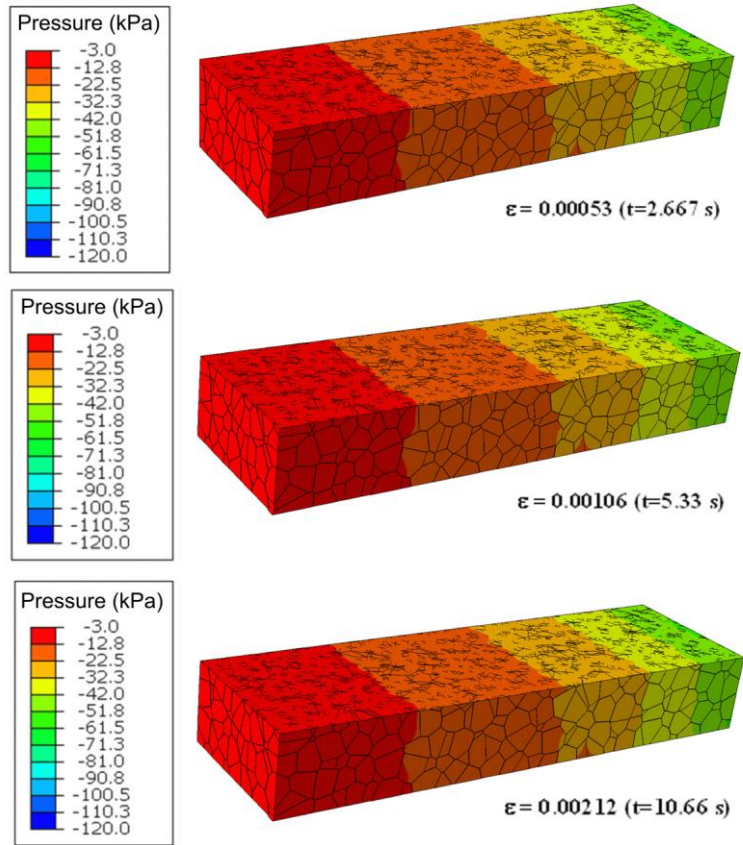


Fig. 7 Contour plots of the liquid pressure for $v_T=90$ mm/min and $\dot{\epsilon} = 0.0002$ s⁻¹ at three different strains. The time of deformation is given in parentheses.